Optimal Lockdown Strategies: All about Time

Anagh Pathak
National Brain Research Centre
Varun Madan Mohan
National Brain Research Centre
Arpan Banerjee (banerjee2007@gmail.com)
National Brain Research Centre

Research Article

Keywords: Lockdown, Optimal temporal window, Infection, SARS-CoV2, Viral spread, Intervention

Posted Date: February 15th, 2021

DOI: https://doi.org/10.21203/rs.3.rs-194973/v1

Optimal lockdown strategies: All about time

Anagh Pathak[1,†], Varun Madan Mohan[1,†], and Arpan Banerjee[1,*]

[1]National Brain Research Centre, Manesar, Gurgaon 122052, India

Abstract

Lockdowns are disease mitigation strategies that aim to contain the spread of an infection by restricting the interactions of its carriers. Lockdowns can thus have a considerable economic cost, which makes the identification of optimal lockdown windows that minimize both infection spread and economic disruption imperative. A well-known feature of complex dynamical systems is their sensitivity to the timing of external inputs. Hence, we hypothesized that the timing and duration of lockdowns should dictate lockdown outcomes. We demonstrate this concept computationally from two perspectives - Firstly, a stochastic "small-scale" Agent Based Model (ABM) of a Susceptible-Infected-Recovered (SIR) disease spread and secondly, a deterministic "large-scale" perspective using a multi-group SIR mass model with parameters determined from the SARS-CoV2 data in India. Lockdowns were implemented as an effective reduction of interaction probabilities in both models. This allowed us to evaluate the parametric variations of lockdown intensity and duration onto the dynamical properties of the infection spread over different connection topologies. We definitively show that the lockdown outcomes in both the stochastic small-scale and deterministic large-scale perspectives depend sensitively on the timing of its imposition and that it is possible to minimize lockdown duration while limiting case loads to numbers below hospitalization thresholds.

Keywords

Lockdown, Optimal temporal window, Infection, SARS-CoV2, Viral spread, Intervention

† Authors with equal contribution, co-first authors

* banerjee2007@gmail.com

Notation

N	Total Population
n_{inf}	Number of individuals initially infected
n_{sim}	Number of simulations
S	Number of susceptible individuals
I	Number of infected individuals
R	Number of recovered/removed individuals
β	Per-individual disease transmission rate
ρ	Re-wiring probability
γ	Recovery rate
r	Number of days for recovery
τ	Lockdown start-time
Δ	Duration of lockdown
p_i	Pre-lockdown coefficient
p_l	Lockdown coefficient
p_{post}	Post-lockdown coefficient
h	Total number of hospital beds
ξ	Maximum fraction of infected individuals
ξ_0	Hospitalization threshold

Introduction

Understanding disease dynamics has assumed vital importance in the midst of the on-going *SARS-CoV2* pandemic. Decision-makers around the world are grappling with the difficult task of weighing the need for lockdown interventions to mitigate disease spread against the negative socioeconomic impact of prolonged disruptions to trade, business and social interactions.[1] Nowhere else is this issue more critically important than in lower income countries (LICs) and lower middle income countries (LMICs), where policy-makers have to decide between imposing strict lockdowns, which inevitably lead to massive financial difficulties for economically weaker sections of the society,[2] or allow the disease to run unchecked and cause a high number of casualties.[3] Therefore, modelling strategies that inform decision-making about the optimum timing and duration of lockdown interventions are the need of the hour.

Despite the considerable economic costs of lockdowns, their design requires comparatively little information about the infectious disease as opposed to pharmaceutical interventions like vaccines. In essence, a lockdown intervention attempts to simply minimise the interaction of entities that are capable of transmitting the pathogen. This makes it impervious to changes in the properties of the pathogen that do not affect its method of transmission. Thus, a well-designed lockdown can be a particularly useful tool for keeping disease spread in check.

Non-linear systems produce differing outputs depending on the timing of application of perturbation.[4,5] For example, neurons in the brain, conceptualized as oscillators that exhibit rhythmic electrical activity, are known to be maximally sensitive to incoming spike currents at specific phases of on-going activity[6] to generate new action potentials (spike). Similarly, cardiac beats are susceptible to respiratory drive at precise phases of the trajectory.[7] Researchers use Phase Response Curves (PRCs) to characterize the effects of external perturbations on system dynamics as a function of the phases at which those perturbations are applied.[8] We conjecture that such insights can be extended to study the effects of lockdown interventions on the on-going dynamics of disease evolution by conceptualizing lockdowns as controlled perturbations of disease spread parameters. Specifically, we hypothesize that the timing of the lockdown intervention would considerably impact lockdown outcomes. This approach has the practical benefit of informing public-health planning to best optimize mitigation strategies in order to minimize lockdown duration while avoiding a catastrophic breakdown of healthcare services like the availability of hospital beds for severe cases.[1]

One relatively new paradigm that seeks to incorporate interactive features of the simulation environment is the agent based modeling (ABM) approach.[9,10] Inspired by Ising and cellular automata models, ABMs regard the system as composed of agents which interact with each other based on well-defined rules.[10] ABMs allow the introduction of environmental and interactive detailing which is not possible in ordinary differential equation based models such as the Susceptible-Infected-Recovered/Removed (SIR) compartmental mass model and its derivatives.[11] For example, with ABMs it is possible to constrain the dynamics to specific graphical topologies such as small-world or scale-free networks, that are often used to model realistic environments such as social networks or cities.[12] Over the past few years, ABMs have been demonstrated to successfully model a

wide variety of realistic systems such as forest ecosystems, financial markets, ant colonies etc.[10,13] Therefore, we first utilize a simple ABM of disease spread dynamics to illustrate the general validity of our assertion that lockdown duration can be optimized.

Subsequently, we demonstrate how the notion of optimal lockdown can exist in a real-world inspired deterministic system. To that end, we employ a realistic age-structured SIR mass model for SARS-CoV2 transmission in India. Contact matrices may be regarded as the network scaffolding on which SIR dynamics evolve; lockdowns are modelled as scaling operations on contact matrices for home, workplaces, school and other sectors. We initially fit the Covid-19 growth curve in India recorded between 30^{th} January, 2020 to 14^{th} July, 2020 using an SIR mass model with relevant model parameters. Next, we use the derived model parameters to explore the parameter space of lockdown timing and duration and produce phase-space trajectories that satisfy relevant criteria.

Thus, using two fundamentally different modelling paradigms, one inherently stochastic and the other deterministic, we demonstrate that the notion of optimal temporal windows for lockdown interventions subject to constraints like hospitalization thresholds is an empirical feature that can be used for understanding and controlling infection outbreaks.

Methods

Model Description

Agent Based Model

We use an Agent Based Model (ABM) defined on a static binary network with pairwise interactions between neighbouring nodes, where the nodes of the network depict individuals in a population and the edges represent relationships between individuals. The underlying social networks that define the interactions between individuals were chosen to be the topologically different Watts-Strogatz small-world network and scale-free networks.[14,15] We generated the small world network by using the ring network rewiring method[14] on a ring network consisting of N nodes and $2 * K = 50$ nearest neighbour edges, with a rewiring probability of ρ. The scale-free networks were generated using the Barabasi-Albert preferential attachment algorithm.[16] The number of nodes and edges were kept comparable across the different topologies to avoid any biases. Initially, the disease is assumed to spread on the above mentioned topology according to the following rules: The total population for a given run is N. At the start of the simulation, n_{inf} nodes are selected at random and designated as *'infected'*. All other nodes are assumed to be *'susceptible'* (**Fig.1**). At each time-step, a single neighbour of an infected node is randomly selected and designated as *'infected'* with an interaction probability (p_i). Once infected, a node is capable of infecting any of its susceptible neighbours, till it recovers. A running counter is maintained throughout the simulation which tracks the number of time steps since infection for all infected nodes. Infected nodes are said to *'recover'* after a given number of time steps have elapsed (r: recovery time), at which point the node ceases to be infectious or capable of getting infected. The lock-down state is a network wide reduction of interaction probability from p_i to p_l and aims to mimic the restriction of interaction of infected nodes. The lockdown starts at τ and is maintained for Δ time-steps. Thus p_l can be considered to be the *mobility* of the population during the lockdown

period and a constraint on the social interaction. Post-lockdown, the interaction probability is maintained at $p_{post} = p_i$. The maximum fraction of infected individuals (ξ) over the entire course of the epidemic serves as an index of lockdown efficacy. The lockdown is considered successful if ξ stays below a specified threshold ξ_0. Due to the stochastic nature of the model, results are averaged over multiple simulation runs (n_{sim}).

Mass model

We employ an age-structured compartmental mass model to fit the SARS-CoV2 infection spread on the Indian population, that can be split into $M = 16$ age-groups ranging from 0-79 years.[17] The contacts among the age groups were classified into four sectors - home (H), school (S), work (W), and other (O).[18] Dynamics of each age-group is captured by the state variables S_i, I_i and R_i which correspond to the number of susceptible, infected, and recovered individuals in the i^{th} age-group (**Fig.7**). The model makes no distinction between recovered or deceased individuals. The dynamics of each age-group is mathematically described by the following ordinary differential equations (ODEs):

$$\dot{S}_i = -\lambda_i S_i \tag{1}$$

$$\dot{I}_i = \lambda_i S_i - \gamma I_i \tag{2}$$

$$\dot{R}_i = \gamma I_i \tag{3}$$

where the effective transmission rate, λ_i, is given by :

$$\lambda_i = \beta \sum_{j=1}^{M} C_{ij} \frac{I_j}{N_j}. \tag{4}$$

C_{ij} is an element of the contact matrix derived through combination of census surveys and Bayesian imputation.[19] C_{ij} is computed as a linear sum of all contact matrices for *Home*, *School*, *work* and *other* places -

$$C_{ij} = C_{ij}^H + C_{ij}^W + C_{ij}^S + C_{ij}^O$$

The model ignores birth and death dynamics and therefore,

$$S_i + I_i + R_i = N_i \tag{5}$$

Lockdowns are modelled as interventions that alter the weights of contact matrices for work, school and other places through coefficients U_W, U_S and U_O :

$$C_{ij}(t) = C_{ij}^H + U_W(t) C_{ij}^W + U_S(t) C_{ij}^S + U_O(t) C_{ij}^O \tag{6}$$

For simplicity we assume $U_W(t) = U_O(t)$ throughout the article. Following[18] we kept the recovery time at 14 days throughout ($\gamma = 1/r = 1/14$). The simulation was initiated with 1 infected individual in the age group 40-44. Euler method was used to integrate the system of 48 ordinary differential equations using an integration time step of 0.1 hr (6 minutes).

To obtain the parameter values to guide further simulations, we fit the simulation against WHO data for the cumulative cases in India till 14^{th} July. The start time for the simulation was kept as 30^{th} January, which also coincided with the start of recorded data. Lockdown imposition was assumed to take place on the 55^{th} day from the start of recording. Lockdown was implemented by altering the weightage of contact matrices with time. Prior to lockdown imposition, lockdown parameter coefficients for the *home*, *work*, *school*, and *other* connectivity matrix were set to 1. Lockdown was assumed to be lifted on the 115^{th} day from the start of the simulation (**Fig.8**). The lockdown state corresponded to reduced coefficients for *work*, *school* and *other* connectivity matrices(< 1). Post-lockdown coefficients for *work* and *other* connectivity matrices were assumed to be higher than their lockdown values, indicating post-lockdown social distancing measures. The lockdown coefficient for *school* was maintained at 0. The lockdown coefficients and per-individual transmission rate (β) were derived from fitting simulation runs to cumulative infection cases recorded till 14^{th} July, 2020[20] (**Fig.8**).

A report by the Center for Disease Dynamics, Economics and Policy (CDDEP), predicts that at its peak, the infection will affect 100 million people in India out of which 2-4 million ($2-4\%$) people will require hospitalization.[21] We use this figure of $2-4\%$ as an estimate of the maximum hospitalization capacity (ξ_0).

The lockdown start time (τ) is varied from 1 to 200 days, and the duration of the lockdown (Δ) is varied from 5 to 200 days. For each simulation, the maximum fraction of infected individuals is computed as :

$$\xi(\tau, \Delta) = \frac{\max\left(\sum_i I_i\right)}{\sum_i N_i}.$$

Assuming the hospitalization capacity to be 3% of the infected cases[21] and that the number of hospital beds in India (public and private sector combined), $h \approx 1.9$ million,[22] we determine the hospitalization threshold (HT) :

$$\xi_0 = \frac{h}{0.03 \times \sum_i N_i} \approx \mathbf{0.0468}$$

The aim of the study is to identify shortest possible lockdown duration that prevents the number of active cases at any given time from exceeding this value. Formally, this corresponds to the condition :

$$\min_{\Delta}\{(\tau, \Delta) \in Z | \xi(\tau, \Delta) < \xi_0) \tag{7}$$

We approach this problem by running the model for $\sum_i N_i = 1353344709$ individuals, divided among the 16 age groups for a duration of 25000 hours to ensure that the disease has run its course. The lockdown functions $U_W(t)$, $U_O(t)$, and $U_S(t)$ are constructed such that its minimum value is 0.3 for U_W and U_O, and 0 for U_S, consistent with the curve fitting exercise (see Results). The non-zero minimum of the lockdown function captures a *leaky* lockdown scenario, which accounts for sectors where activity cannot be completely arrested, in spite of strict implementation. The lockdown functions are thus defined as :

$$U_W(t) = U_O(t) = \begin{cases} 1\ (p_i) & \text{if } t < \tau \\ 0.3\ (p_l) & \text{if } t >= \tau\ \ \&\ \ t < \tau + \Delta \\ p_{post} & \text{if } t >= \tau + \Delta \end{cases}$$

$$U_S(t) = \begin{cases} 1\ (p_i) & \text{if } t < \tau \\ 0\ (p_l,\ p_{post}) & \text{if } t >= \tau \end{cases}$$

The Δ satisfying equation(7) can be found by thresholding ξ at ξ_0 (**Fig.9.**). In order to illustrate the effect of the post-lockdown coefficients on optimal lockdown strategies, we carry out this exercise for $p_{post} = 0.75$ and $p_{post} = 1$ (full reopening of the *work* and *other* contact matrix) as well (**Supplementary Fig. S1 and S2**).

Results

Optimal lockdown in agent based model of disease spread over small-world and scale-free topologies

We used the agent based model (ABM) to simulate the evolution of susceptible, infected and recovered populations during disease spread[23] on network nodes with small-world and scale-free connection topologies. The number of infected individuals in the population grows over time until it reaches a critical value (**Fig.1**) for both networks. Thereafter, we notice a reduction in the number of cases (infected population). Depending on the model parameters, ξ could be as high as 1, implying that the disease has infected all individuals in the population (**Fig.1**). **Figure 1** also shows the fraction of susceptible, infected and recovered individuals at different time-points of infection spread for small-world and scale-free networks.

Lockdown scenarios could be captured by parametric control of the lockdown interaction probability (p_l) in ABM evolution. **Figure 2** demonstrates the effect of lockdown on disease spread (in boxed regions A, B and C). For the particular case depicted in the figure (d=30 days), we observe the existence of 3 qualitatively different scenarios. For an early lockdown (day 1), we find that ξ is considerably smaller than what would have happened without a lockdown. For a slightly delayed start (day 10), infection is arrested during the lockdown period, but there is an emergence of a peak post lockdown period. Finally, if there is a late lockdown start (day 19), ξ reaches almost same levels as without interventions. Furthermore, we also find that a smaller duration of early lockdown cannot prevent ξ to reach almost the same levels of that without intervention and the existence of an optimal region (around day 9) where a relatively short lock-down is able to control the spread of the infection.

Lockdown mobility: Lower values of the parameter mobility gave more favorable outcomes, i.e, reduction in ξ for a wider range of lockdown start time and duration (**Fig.3**). However, with increases in mobility (upto 0.1), we observed the size of the optimal region where a slightly delayed lock-down can achieve better results than an early lockdown. The similar pattern was observed for both small-world and scale-free networks.

Network topology and population size: **Figure 3** also suggests differences in lockdown outcomes for the two network topologies considered here, with disease spreading more aggressively on small-world topologies. An equally relevant parameter for social-networks is the overall size. Qualitatively similar results were obtained for bigger populations, as evidenced by **Fig.4** (N= 10000), however the number of active cases peaked much later($\approx$ 15 days) as compared to smaller population sizes.

Recovery time: The recovery time (r) of the infection has a considerable effect on lockdown efficacy in both network topologies, as shown in **Fig.5**. A higher recovery time increases the overall severity of the epidemic, as is suggested by ξ values. Interestingly with higher recovery times, the parameter space where an early lockdown with long duration would have inadvertently controlled the epidemic shrinks rapidly. Subsequently, the optimal regions where timing of a lockdown is a crucial parameter to consider emerges as the best intervention.

Optimal lockdown windows: We further evaluated how the existence of optimal lockdown windows change when rewiring probability is varied in small-world and scale-free networks. For small-world graphs, higher ξ values were observed for larger values of the rewiring probability (**Fig.6**). In **Fig.3, 5**, and **6**, it is interesting to note that the location of the optimal temporal window post which lockdown interventions are rendered futile remains in the vicinity of day 9. **Figures 3, 4, 5,** and **6** clearly show that a lockdown scenario characterised by simply reducing the probability of interaction of the infected nodes with their neighbours can have a drastic effect on the severity of the epidemic on any given day. However, a lockdown event, although resulting in a low ξ, can result in more than one infection event, as illustrated in **Fig.2**. Nonetheless, since ξ is the global upper bound on the number of individuals infected throughout the course of the epidemic, it is ideal for gauging the effectiveness of the lockdown strategy. The similar location of the optimal temporal window in **Fig.2, 3, 5, 6** indicate that this feature does not depend on the structure of the network, or on the recovery time. This effect was also observed in the larger networks, albeit around day 14/15 (**Fig.4**). Post this window, all lockdown strategies are rendered nugatory, no matter how long the duration of the lockdown. This alludes to the possibility of the unhindered disease crossing a certain threshold, after which it becomes impossible to arrest the infection spread using any kind of lockdown strategy. Comparison of the location of the observed temporal window with an unhindered epidemic, for both N=1000 and N=10000 suggests that this threshold lies at around $S = 0.68 * N$, where S is the number of susceptible individuals.

Optimal lockdowns in multi-group mass model

We observe the characteristic features of the SIR dynamics from our model parametrized by realistic parameters (**Fig.8**). The number of active cases increase exponentially at first, reaches a peak and subsequently, falls off. The point at which the unmitigated spread of infection reaches its peak is regarded as the herd-immunity threshold (HIT). The number of recovered individuals increases over time and saturates when the disease spread is terminated.

Lockdown scenarios are modelled by altering lockdown functions U_W, U_S and U_O during and after the lockdown (**Fig.8, 9**). Since schools were shut down during the lockdown and remain shut even 7 months after the formal lifting of nation-wide lockdown in India, we assume $U_S = 0$ for all times after lockdown start. We find the best fit to actual data by assuming $\beta = 0.013$, and $U_W = U_O = 0.3$ during the lockdown and $U_W = U_O = 0.45$ after the lockdown (**Fig.8**).

Optimal temporal windows for lockdown: Lockdown parameter space is explored by varying lockdown start time and duration (**Fig.9**). The lockdown functions were assigned values derived from fitting the model against actual data recorded from 30th January to 14th July[20] (**Fig.8**). The maximum number of active cases computed for each lockdown parameter configuration was compared to numbers that can be maximally catered by the hospital infrastructure and used as a measure of the strain on hospital capacity. As the heatmaps (**Fig.9**) clearly indicate, there exists considerable variability in lockdown outcomes as a function of start times and duration. For example, case A (**Fig.9**) ($\tau = 81$, $\Delta = 65$) results in the active infections surpassing the hospitalization threshold (HT),

ξ_0. Similarly, case C illustrates that late lockdowns ($\tau = 120$, $\Delta = 65$) also result in a violation of the HT. However, the same lockdown duration as A & C implemented around the 101^{st} day prevent the active cases from breaching the HT. This phenomenon, which results from the non-linearity inherent in SIR dynamics, is easily visualized by plotting disease trajectory in the phase space(S vs I) (**Fig.9**). The optimal lockdown window that prevents a breach of the HT can also be found in the cases where post-lockdown values of U_W and U_O are set to 0.75 or 1 (**Supplementary Fig. S1 and S2**). However, in these cases, the minimum duration of a favourable lockdown strategy is considerably greater (100 days and 135 days for $U_W = U_O = 0.75$ and 1 respectively).

Discussion

The SARS-CoV2 outbreak has triggered concentrated interest in epidemiological modelling of viral infection spread.[24] The primary aim of these studies is to suggest an informed and logical response to disease spread via socio-dynamic interventions.[1,3,25] Our study is distinct in its aims to understand the possible players in this complex dynamical system that can be validated from empirical data. Lockdown timing is one such parameter which can perturb the dynamic system such that the attractor landscape is altered favorably. We demonstrate this initially using a rule-based stochastic viral spreading model through agent based modelling (ABM) on small-world and scale-free connection topologies. Subsequently, we demonstrate that the optimal windows can exist in the well established compartmental mass model that currently is used worldwide for planning lockdowns.[11,24] While, qualitatively the disease spreads appear to resemble the ODE-based SIR-models,[26] ABMs provide more flexibility in adding real-world complexity and simulations of interventions. Even though one can argue that the growth of SARS-CoV2 is relatively less in some countries including India, we believe this understanding is crucial for future outbreaks as well as to arrest disease progress in local communities. In the remainder of this section, we discuss the features of the disease spread in the face of various lockdown strategies, in the two modelling paradigms, describing features unique and common to each paradigm. We also stress on the importance of lockdown parameters as intervention strategies to viral outbreaks.

ABM as a tool to plan optimal lockdown

ABM was employed on a static network with nodes that have only one attribute - its disease state (susceptible, infected, or recovered). The parameters in this model can be broadly classified as (*i*) Network parameters - node number, degree distribution, and the graph architecture, (*ii*) Agent parameters - mobility (interaction probability), number of interactions per day, and (*iii*) Disease parameters - infection probability, recovery time. Based on such a simplified parameter space we could simulate the complex dynamics of the disease spreads and study the effects of lockdown scenarios. One key result of our work is the existence of the optimal temporal windows for lockdown efficacy that can exist due to interaction of disease parameters and network topology. Second, we could demonstrate systematic differences in the severity of disease spread (as indexed by ξ) between small-world and scale-free networks (**Fig.1**). Third, our ABM analysis reveals that early lockdowns may not be as efficacious because they limit the beneficial effects of herd-immunity and therefore risk the possibility of secondary waves of infection after the lockdown is lifted. Finally, the size of the population is found to be an important determinant to place the location of optimal lockdown windows (**Fig.4**).

A clear outcome of the ABM analysis is that optimal lockdown windows exist and depend sensitively on topological (network architecture) and social factors (mobility), as well as on the inherent disease parameters (e.g. recovery time). It is apparent that imposing early lockdowns is no guarantee against adverse outcomes, as premature lockdowns limit the influence of herd-immunity and thereby do not preclude the possibility of aggressive post-lockdown spread. The problem is exacerbated by the *leakiness* inherent to any lockdown intervention as it is practically impossible to completely arrest activity in a real-world scenario. Indeed, our model is capable of predicting the possibility of

second-waves due to ineffectual lockdowns.[27] It is also apparent that delayed imposition of lockdowns lead to a breakdown of essential medical services, thereby leading to **high death rates**. Counteracting the effect of the delay would require untenable lockdown durations. Our model predicts the existence of brief periods, close to the peak of the spread, that present windows where even moderate lockdown durations can drastically reduce the size of subsequent infection peaks.

An important observation from the ABM analysis is that small-world networks seem to be worse affected by disease spreads in terms of ξ. However, the concerted effect of lockdown on both the networks is almost identical. The reason for this result can be arrived at by looking at the parameters that affect disease transmission in a network in relation to the lockdown strategy employed. A lockdown is an intervention which alters the usual course of the epidemic by abruptly reducing the probability of infection spread by restricting the interactions of infected individuals while not affecting the change in the structure of neighbourhoods in both types of networks. Thus, the lockdown can be viewed as a control of dynamics on a given set of structural constraints but not directly affecting the interaction properties between nodes. The effect of reducing interaction probability to various values of p_i is clearly shown in **Fig.3**. The default value of p_i is 0.5, which implies that an infected node has a fifty percent chance of interacting with a randomly chosen neighbour. Naturally, reducing this value of p_i to the extreme value of 0 would imply that an infected node interacts with absolutely no neighbour throughout the lockdown. In this case, if the duration of the lockdown is such that it exceeds the recovery time of the disease, the infection would die out. Such extreme values of p_i seem implausible in a real-world setting, and so we assume non-zero values of p_l, or *"leaky lockdowns"*. The lowest value of p_i used in this study is 0.001, which is low enough to render even a 10-day lockdown highly efficacious, as long as it is implemented early enough. As p_l is increased, we see that lockdowns of small duration are not efficacious even if implemented at an early stage (**Fig.2**).

Simulation results indicate the peak in active cases occurs later for larger as compared to smaller populations for the same number of local connections (**Fig.4**). This is a crucial consideration while comparing lockdown timings between countries with different population sizes. Interestingly, the optimal lockdown timing seems to shift between N = 1000 and N= 10,000 **(Fig.4)**. This change could be explained by observing that the mean degree for both N = 1000 and N = 10,000 is kept at $\overline{K} = 50$ and therefore, the spreading dynamics is delayed for the case of larger population. One could expect $\overline{K}$ to scale with population size, but research has suggested that the local contact rate remains constant across larger and smaller populations.[11]

Optimal lockdown windows in realistic scenarios using mass modelling

In response to the global SARS-CoV2 pandemic, the Government of India imposed a 4 phase nation-wide lockdown that lasted from 25^{th} March, 2020 to 31^{st} May, 2020. This was followed by 2 phases of *unlocks*, with the second unlock phase still underway at the time of writing. While being a necessary step to ensure disease mitigation, the lockdown brought tremendous hardship to the economy, causing disruption in livelihoods, supply-chains and stalling growth.[28,29] These factors ultimately led to calls for lifting of the

lockdown. We adapted our previous analysis to actual data in order to estimate optimal lockdown windows such that, (i) the maximum number of active cases in the resulting dynamics remain lower than the total hospitalization capacity, and (ii) condition (i) is satisfied for the smallest possible lockdown duration. As argued before, such a solution ensures medical assistance to the most severe cases, while keeping the economic fallout of a protracted lockdown to a minimum. India is credited with imposing one of the most stringent lockdowns as measured by the lockdown stringency index devised by the Oxford University.[30] Inspite of this, the lockdown period coincided with an increase in overall case loads[31] (**Fig.8**). Therefore, we regarded lockdown intensity as an important criteria that demands explicit factoring into any realistic model to assess lockdown scenarios.

For sake of simplicity, we restricted ourselves to one-shot, square-wave like lockdown functions, such that the only relevant lockdown parameters were the start-time, duration and intensity of the lockdown. We use an age-structured SIR model to fit actual data (cases and lockdown times) in order to estimate relevant parameters— per-individual transmission rate (β) and lockdown intensity during and after the lockdown implementation (**Fig.8**). Even a simple SIR model with realistic age-based compartmentalization gives rise to rich dynamics due to the non-linearity inherent in equations (1) and (2). This richness is manifested in the sensitive dependence of outcomes of mitigation strategies on the timing and duration of the lockdown. This effect can be intuitively understood as arising from the interaction of lockdown measures and herd-immunity thresholds (HITs) (**Fig.9**). Early lockdowns doubtless lead to immediate cessation of disease spread. However, early lockdowns make a second wave of infection inevitable because the number of susceptible individuals in the population after the lockdown remains comparable to the number of susceptible individuals at the start of the pandemic, far from the HIT of the system. In this scenario, infections climb again once the lockdown is lifted.[25,32] Therefore, such lockdowns do not lead to good long-term outcomes as the second wave of the infection easily takes the number of active cases past the hospitalization threshold (HT). On the other extreme, as with the ABM, late lockdowns do not help either as the worst phase of the epidemic is already over at this point and the HTs have already been breached. Therefore, it is evident that the most suitable solutions that prevent medical infrastructure overload, while reducing the lockdown duration, lie somewhere in the middle. Successful lockdown strategies leverage the mitigatory effects of lockdowns along with inherent HITs (beyond which the number of infected individuals strictly decrease). As argued in the Introduction, such effects can be likened to phase resetting curves in neuroscience, where this concept is used to estimate the probability of neural spiking as a function of the timing of an external perturbation.[6,8]

We conclude by laying out the inherent assumptions and possible limitations of the SIR model. Firstly, our model ignores temporal delays that are likely to exist between lockdown announcement and effective implementation. We think that such delays would not amount to substantial differences in disease dynamics as it is possible that the effects of the delay are offset by a gradual reduction in social mobility preceding the actual lockdown announcement. Additionally, this assumption simplifies the model considerably. Certainly country specific delays would change the predictions from the model. Secondly, by assuming a single value for ξ_0, the model implicitly assumes spatial homogeneity in the distribution of medical infrastructure across the country. However, both disease burden and medical infrastructure is known to be heterogeneously distributed across

the country.[21] Detailed modelling at the level of individual states and districts could potentially solve the problem but at considerable computational costs. We decided to favour model simplicity since our focus was on assessing optimal lockdown scenarios. Thirdly, it is well-known that the number of reported cases is a function of the number of tests conducted. Our model does not account for fluctuations in the rate of testing that may influence the total number of infected individuals at any given time. Further we don't account for the inherent birth and death rates of the population during the course of the infection. Lastly, existence of optimal lockdown windows depends upon the choice of the quantity that we are aiming to optimize. The current analysis places a premium on the maximum fraction of infected individuals (ξ), which serves as a measure of strain on the medical infrastructure at any given point of time. Indeed, recent events have demonstrated the need for *curve flattening* in order to de-congest hospitals and reduce the burden on health-care professionals. However, it may be useful to frame the problem within a formal optimization framework to optimize quantities derived from other economic considerations.[32]

Data availability

The datasets generated during and/or analysed during the current study, and codes for analysis are available from the corresponding author on reasonable request.

References

[1] Moser, C. A. & Yared, P. Pandemic lockdown: The role of government commitment. Tech. Rep., National Bureau of Economic Research (2020).

[2] Singh, M. K. & Neog, Y. Contagion effect of covid-19 outbreak: Another recipe for disaster on indian economy. *Journal of Public Affairs* e2171 (2020).

[3] Lancet, T. India under covid-19 lockdown. *Lancet (London, England)* **395**, 1315 (2020).

[4] Shulgin, B., Stone, L. & Agur, Z. Pulse vaccination strategy in the sir epidemic model. *Bulletin of mathematical biology* **60**, 1123–1148 (1998).

[5] Nie, L., Teng, Z. & Torres, A. Dynamic analysis of an sir epidemic model with state dependent pulse vaccination. *Nonlinear Analysis: Real World Applications* **13**, 1621–1629 (2012).

[6] Canavier, C. C. Phase response curve. *Scholarpedia* **1**, 1332 (2006). Revision #91651.

[7] Kralemann, B. *et al.* In vivo cardiac phase response curve elucidates human respiratory heart rate variability. *Nature communications* **4**, 1–9 (2013).

[8] Schultheiss, N. W., Prinz, A. A. & Butera, R. J. *Phase response curves in neuroscience: theory, experiment, and analysis* (Springer Science & Business Media, 2011).

[9] Crooks, A. T. & Heppenstall, A. J. Introduction to agent-based modelling. In *Agent-based models of geographical systems*, 85–105 (Springer, 2012).

[10] Bonabeau, E. Agent-based modeling: Methods and techniques for simulating human systems. *Proceedings of the national academy of sciences* **99**, 7280–7287 (2002).

[11] Hethcote, H. W. The mathematics of infectious diseases. *SIAM review* **42**, 599–653 (2000).

[12] Eubank, S. *et al.* Modelling disease outbreaks in realistic urban social networks. *Nature* **429**, 180–184 (2004).

[13] Tisue, S. & Wilensky, U. Netlogo: A simple environment for modeling complexity. In *International conference on complex systems*, vol. 21, 16–21 (Boston, MA, 2004).

[14] Watts, D. J. & Strogatz, S. H. Collective dynamics of 'small-world'networks. *Nature* **393**, 440 (1998).

[15] Albert, R. & Barabási, A.-L. Statistical mechanics of complex networks. *Reviews of modern physics* **74**, 47 (2002).

[16] George, M. B-a scale-free network generation and visualization. *Matlab Central* **12** (2006).

[17] Desa, U. United nations department of economic and social affairs, population division. world population prospects: The 2015 revision, key findings and advance tables. In *Technical Report: Working Paper No. ESA/P/WP. 241* (2015).

[18] Singh, R. & Adhikari, R. Age-structured impact of social distancing on the covid-19 epidemic in india. *arXiv preprint arXiv:2003.12055* (2020).

[19] Prem, K., Cook, A. R. & Jit, M. Projecting social contact matrices in 152 countries using contact surveys and demographic data. *PLoS computational biology* **13**, e1005697 (2017).

[20] WHO. *WHO Coronavirus Disease Dashboard* (2020 (accessed July 14, 2020)). URL `https://covid19.who.int/?gclid=EAIaIQobChMIz_CYuYTe6gIV1zMrCh3hOAlUEAAYASAAEgJapPD_BwE`.

[21] Klein, E. *et al. COVID-19 for India updates*. Ph.D. thesis, Princeton University (2020).

[22] Kapoor, G. *et al.* State-wise estimates of current hospital beds, intensive care unit (icu) beds and ventilators in india: Are we prepared for a surge in covid-19 hospitalizations? *medRxiv* (2020).

[23] Newman, M. *Networks* (Oxford university press, 2018).

[24] Dehning, J. *et al.* Inferring change points in the spread of covid-19 reveals the effectiveness of interventions. *Science* (2020).

[25] Malani, A. *et al.* Adaptive control of covid-19 outbreaks in india: Local, gradual, and trigger-based exit paths from lockdown. Tech. Rep., National Bureau of Economic Research (2020).

[26] Kermack, W. O. & McKendrick, A. G. Contributions to the mathematical theory of epidemics—i. *Bulletin of mathematical biology* **53**, 33–55 (1991).

[27] Xu, S. & Li, Y. Beware of the second wave of covid-19. *The Lancet* **395**, 1321–1322 (2020).

[28] Dev, S. M., Sengupta, R. *et al.* Covid-19: Impact on the indian economy. *Indira Gandhi Institute of Development Research, Mumbai April* (2020).

[29] Buheji, M. *et al.* The extent of covid-19 pandemic socio-economic impact on global poverty. a global integrative multidisciplinary review. *American Journal of Economics* **10**, 213–224 (2020).

[30] Hale, T., Webster, S., Petherick, A., Phillips, T. & Kira, B. Oxford covid-19 government response tracker. *Blavatnik School of Government* **25** (2020).

[31] Pulla, P. Covid-19: India imposes lockdown for 21 days and cases rise (2020).

[32] Rachel, L. An analytical model of covid-19 lockdowns. *Author website* (2020).

Acknowledgements

This work was supported by NBRC core funds and the NBRC Computing Facility.

Author contributions

A.P., V.M.M., and A.B. wrote the main manuscript text and A.P. and V.M.M. prepared the figures. All authors reviewed the manuscript.

Additional Information

Competing interests

The authors declare no competing interests.

Figure Legends

$N_I = 10$ and $n_t = 5$ for all the cases unless otherwise stated.

Figure 1. Agent based SIR model

Disease spread on **(a)** Scale-free **(d)** Small-world networks, with $N = 700$ and $\overline{K} \approx 20$; **(b)** and **(c)** describe the SIR dynamics for the networks in (a) and (d) respectively.

Figure 2. Lockdown scenarios

3 lockdown scenarios for small-world *(left)* and scale-free *(right)* network $N = 1000$, $\overline{K} \approx 50$ and $p_l = 0.05$. Heatmap color indicates ξ for different values of lockdown start time τ and duration Δ.

Figure 3. Effect of mobility during lockdown

(a) ξ for small-world networks with various values of lockdown mobility p_l **(b)** ξ for scale-free networks. $N = 1000$, $\overline{K} \approx 50$, $r = 10$

Figure 4. Effect of population size

(a) ξ for $p_l = 0.05$ and $p_l = 0.1$ for small-world and **(b)** scale-free networks for $N = 10,000$.

Figure 5. Effect of recovery time

ξ as a function of recovery time, r for **(a)** small-world and **(b)** scale-free topology.

Figure 6. Effect of re-wiring probability

ξ for various rewiring probabilities ρ and scale-free network. $\overline{K} \approx 50$.

Figure 7.

Contact structures and age-demographics of India: (a) Model schematic, every age group is modelled as a SIR population coupled through contact matrices for home, work, school and other places. **(b)** Population split into 16 age groups from 0-79. **(c)** contact matrices for Home, work, school and others respectively, plotted as heatmaps. Normalized colorbar indicates magnitude of interaction between age-groups.

Figure 8.

Model fitting from empirical data (a) SIR dynamics for model with $\beta = 0.013$,$U_W = U_O = 0.3$ during lockdown and $U_W = U_O = 0.45$ post lockdown. The number of active infected cases peaks on the 346^{th} day since the beginning of the lockdown. **(b) Inset:** *(Top)* Model fit to cumulative infected cases in India— red indicates WHO data, blue indicates model fit. Lockdown is assumed to have started on 25^{th} March and lifted on 31^{st} May. Model parameters were estimated with data collected till 14^{th} July. *(Bottom)*

Model derived lockdown functions for Work, School and Others. Lockdown function for home was considered to be 1 throughout.

Figure 9.

Characterizing lockdowns: Heatmap shows the maximum number of active cases as fraction of total population for model runs with varying lockdown start time (τ, days since start of spread) and duration (Δ, in days). **a-c** indicate the phase trajectories for lockdown strategies marked in the heatmap, along with the corresponding lockdown functions*(right panel)*. The red horizontal broken lines in **a-c** indicate the hospitalization threshold and the blue vertical lines mark the Herd-Immunity Threshold (HIT) beyond which the number of active cases are assured to fall. **b** shows that it is possible to restrict active cases below the hospitalization threshold for the given lockdown parameters. The lockdown function is derived from fitting the model with WHO data.

Figures

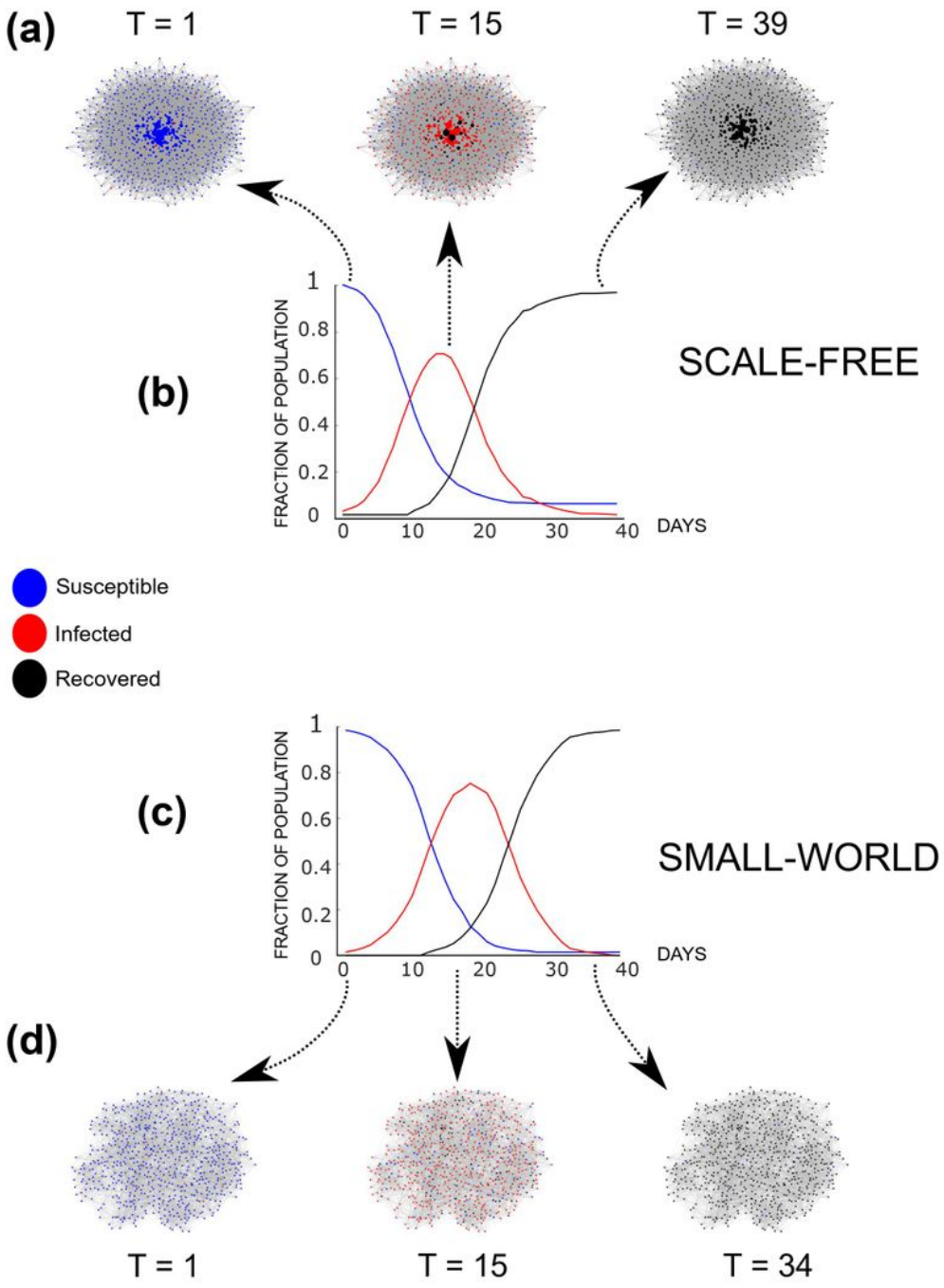

Figure 1.

Figure 1

Please see the Manuscript PDF file for the complete figure caption

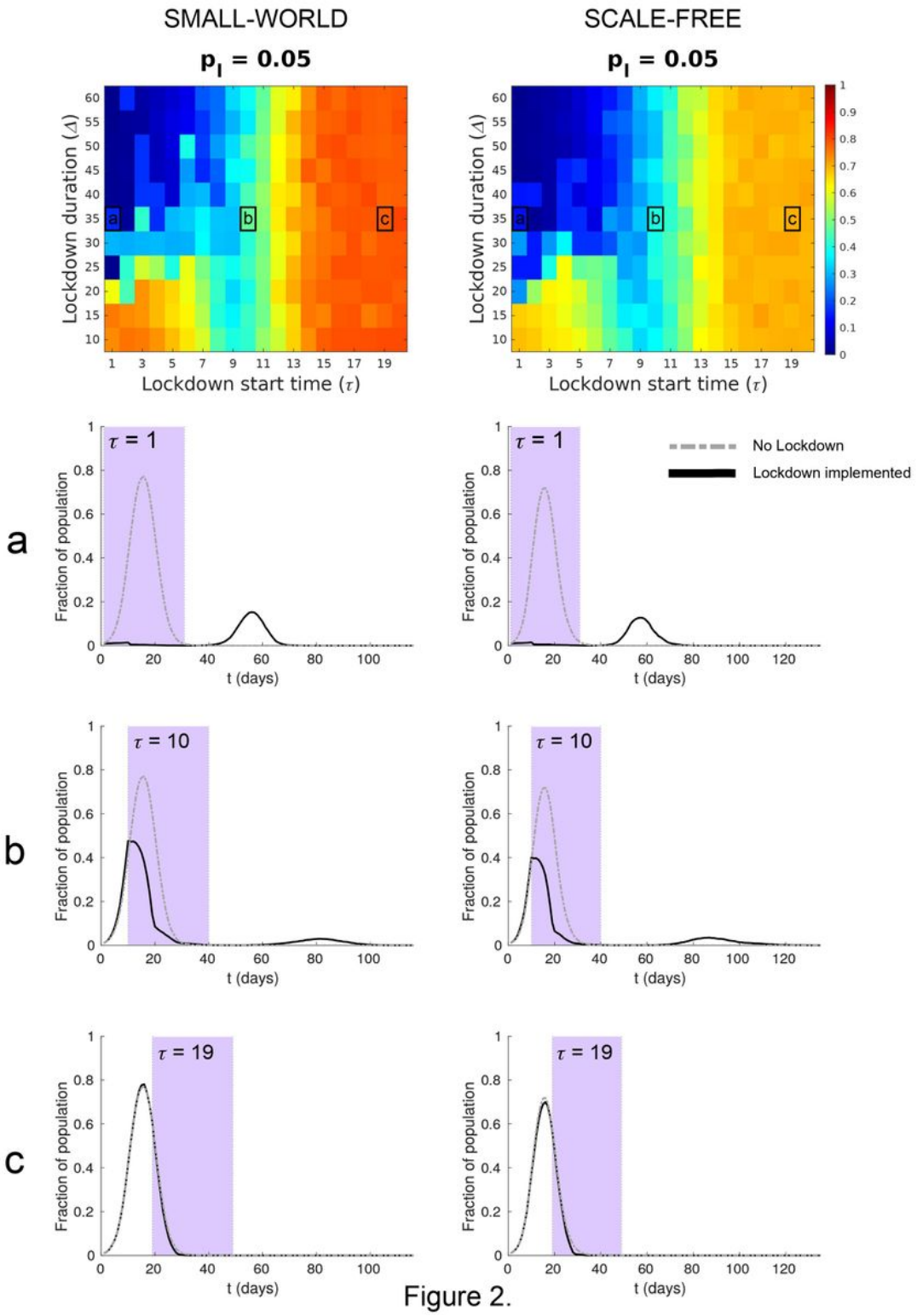

Figure 2.

Figure 2

Please see the Manuscript PDF file for the complete figure caption

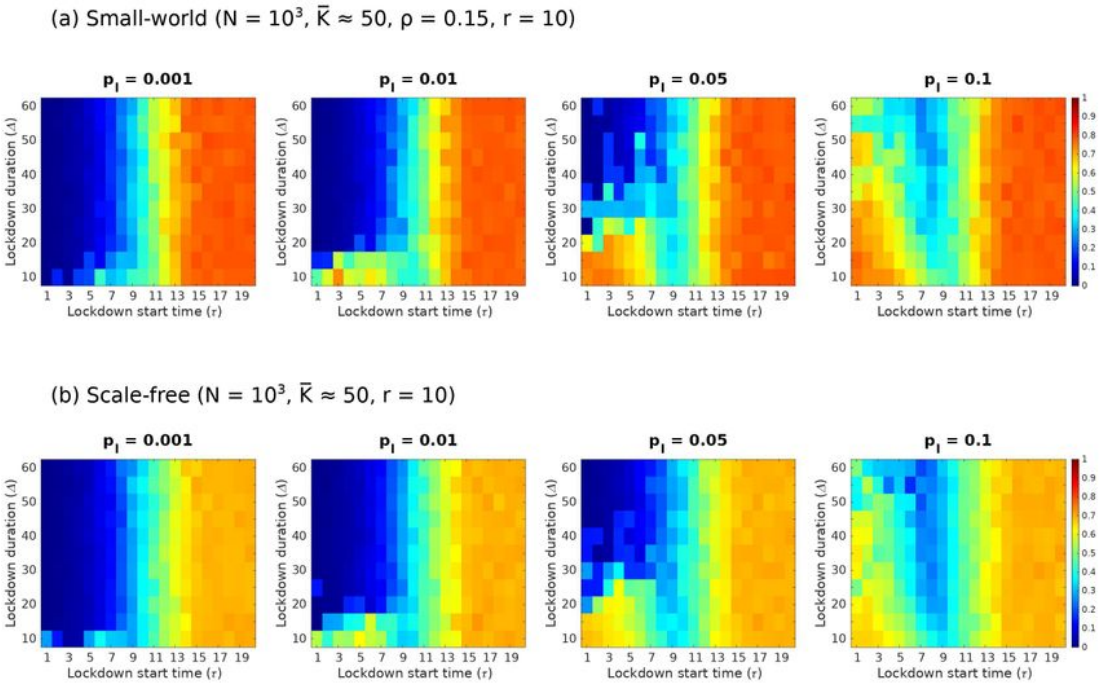

Figure 3.

Figure 3

Please see the Manuscript PDF file for the complete figure caption

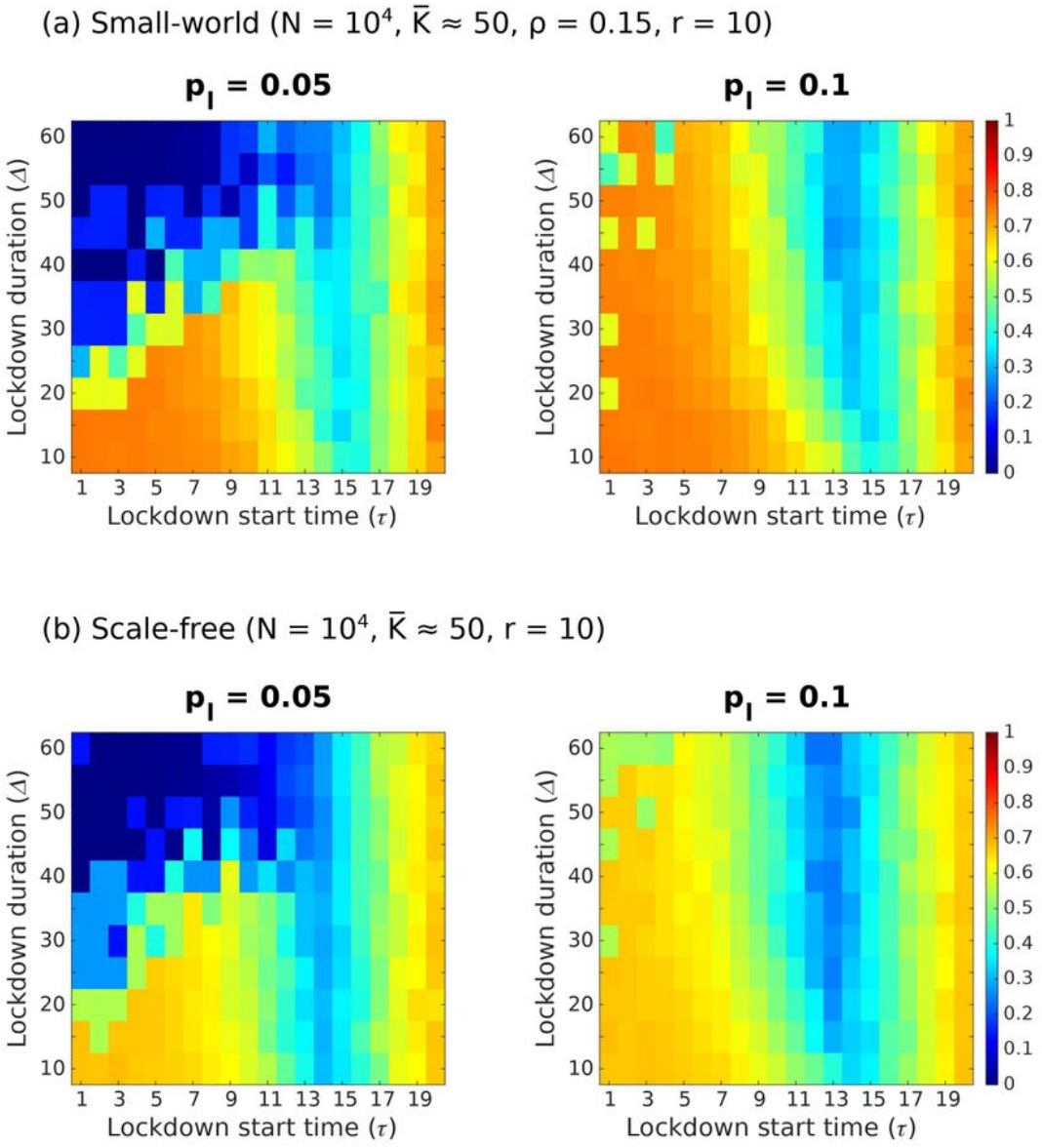

Figure 4.

Figure 4

Please see the Manuscript PDF file for the complete figure caption

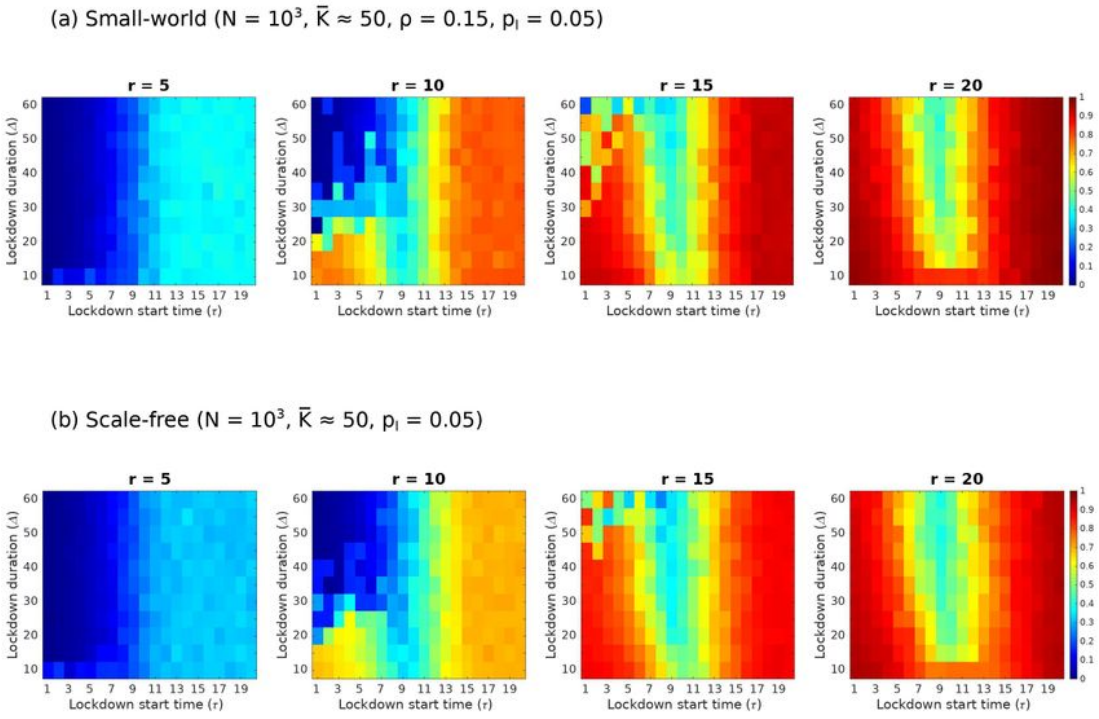

Figure 5.

Figure 5

Please see the Manuscript PDF file for the complete figure caption

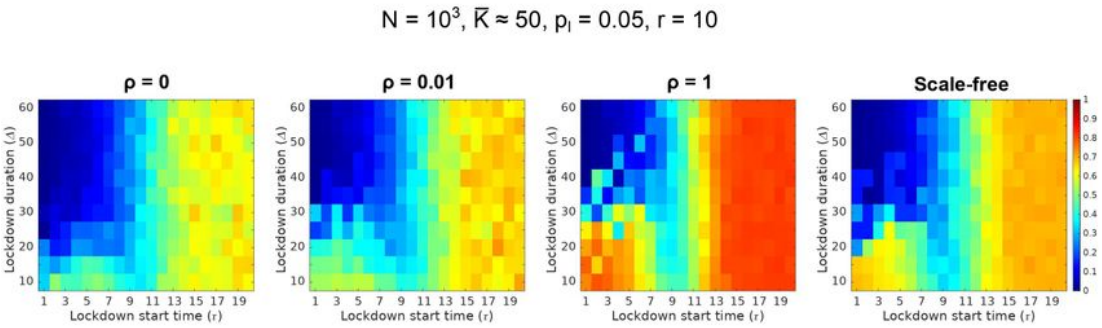

Figure 6.

Figure 6

Please see the Manuscript PDF file for the complete figure caption

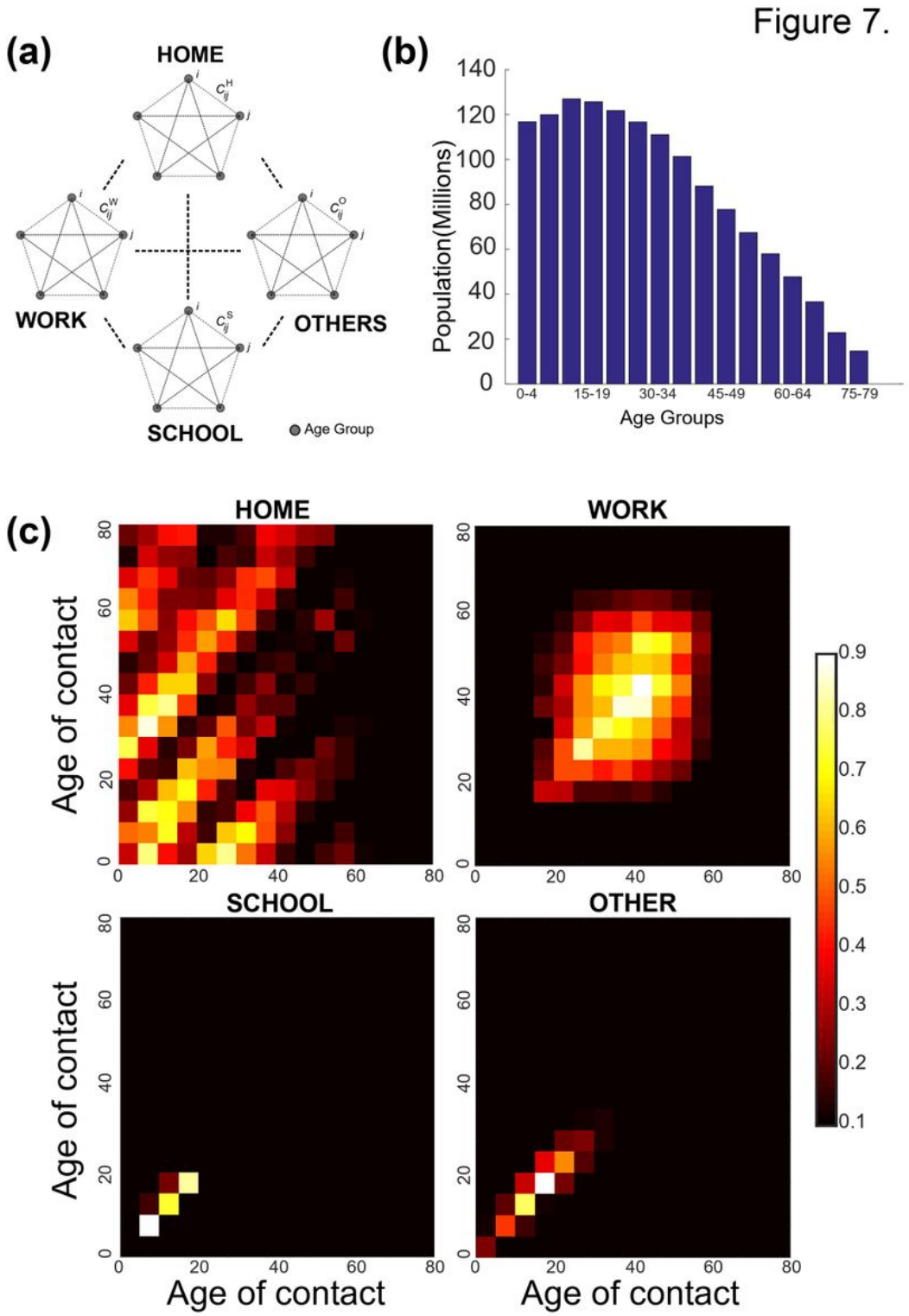

Figure 7

Please see the Manuscript PDF file for the complete figure caption

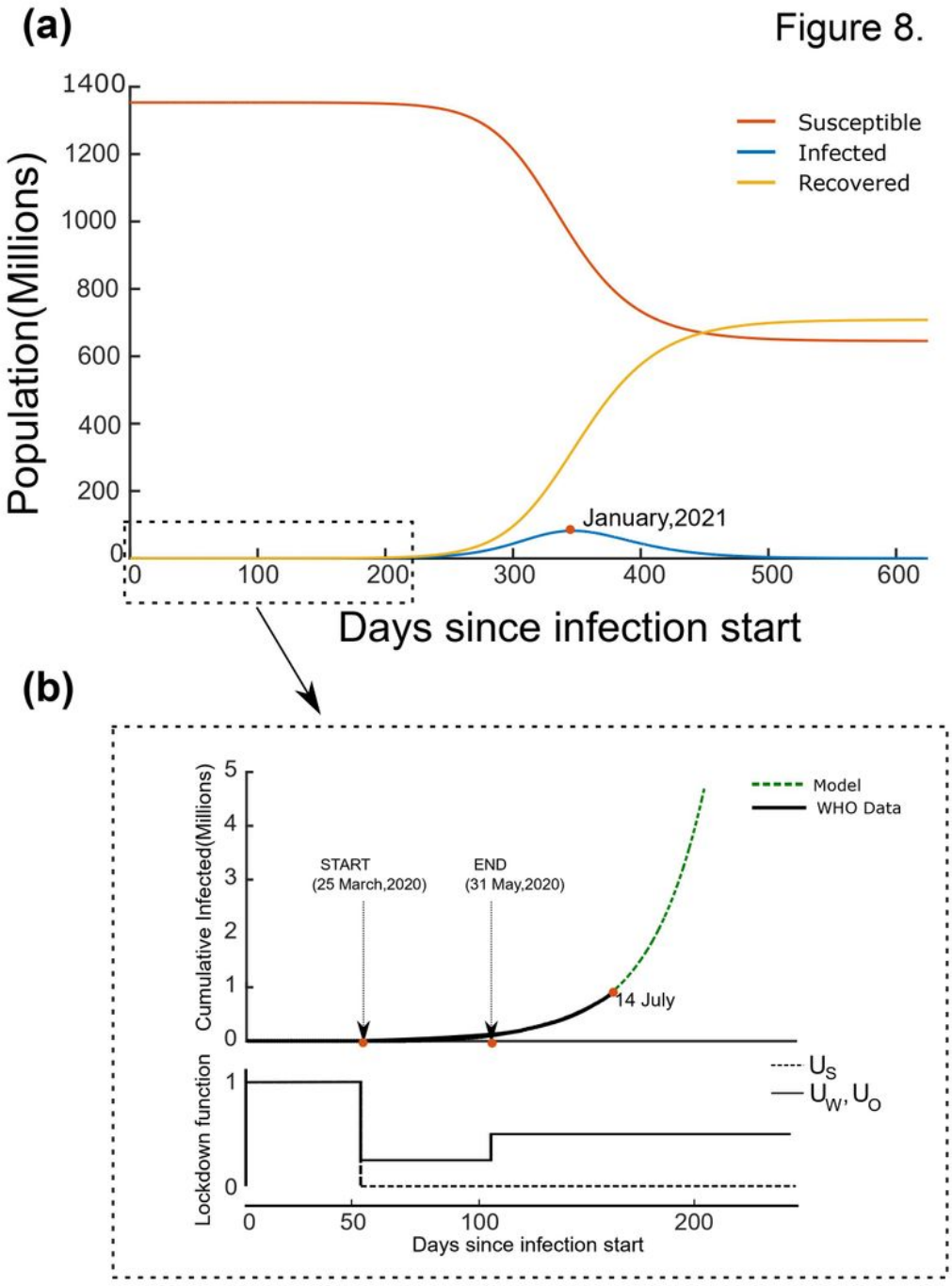

Figure 8

Please see the Manuscript PDF file for the complete figure caption

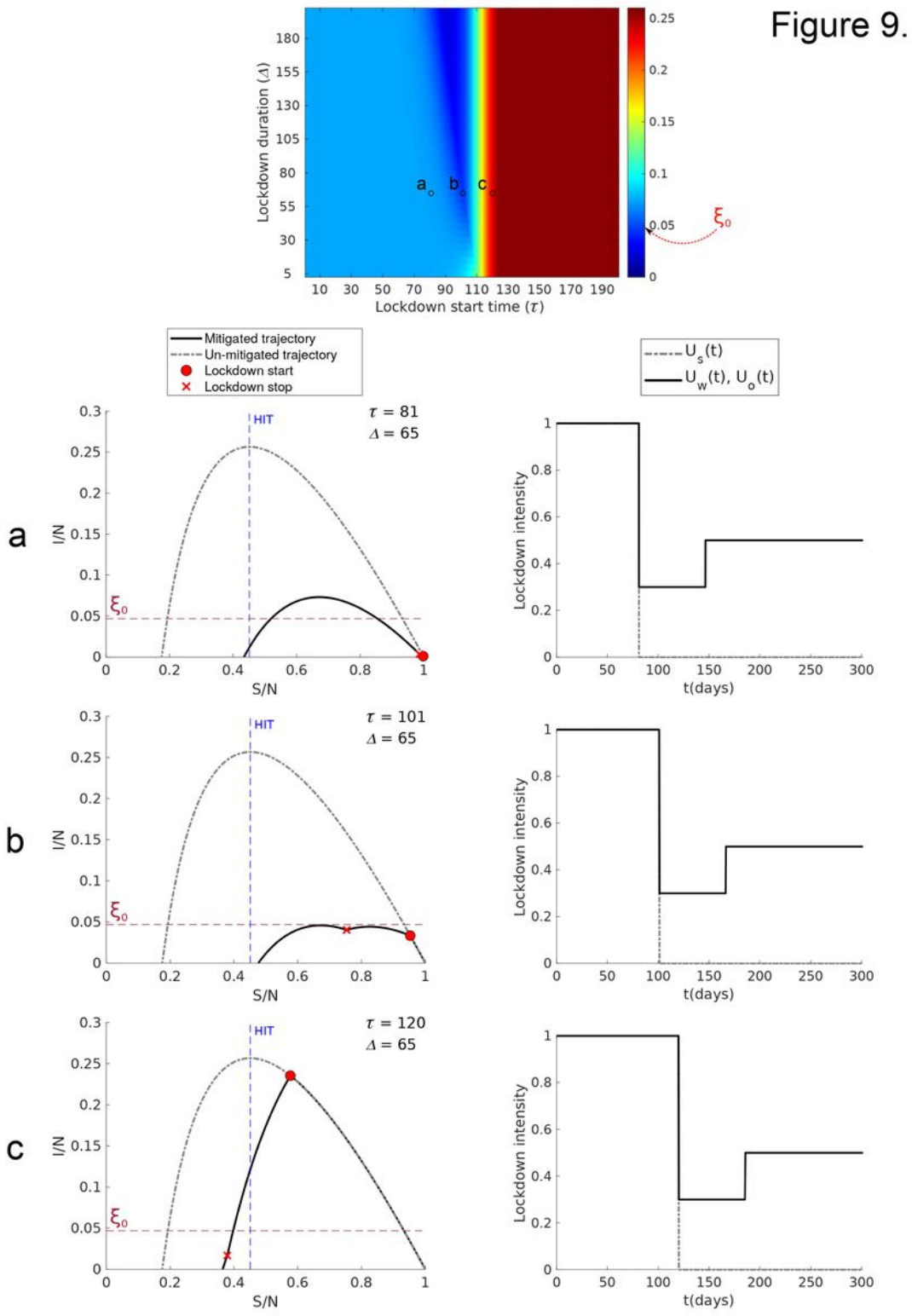

Figure 9

Please see the Manuscript PDF file for the complete figure caption

Supplementary Files

This is a list of supplementary files associated with this preprint. Click to download.

- suppinfoscirep.pdf